BRIEF COMMUNICATION
https://doi.org/10.1038/s43588-022-00297-y

nature computational science

Effective lifetime of non-equilibrium carriers in semiconductors from non-adiabatic molecular dynamics simulations

Shanshan Wang[1,2,8], Menglin Huang[1,8], Yu-Ning Wu[2], Weibin Chu[3], Jin Zhao[4], Aron Walsh[5], Xin-Gao Gong[3,6], Su-Huai Wei[7] and Shiyou Chen[1,2,3] ✉

The lifetimes of non-equilibrium charge carriers in semiconductors calculated using non-adiabatic molecular dynamics often differ from experimental results by orders of magnitude. By revisiting the definition of carrier lifetime, we report a systematic procedure for calculating the effective carrier lifetime in semiconductor crystals under realistic conditions. The consideration of all recombination mechanisms and the use of appropriate carrier and defect densities are crucial to bridging the gap between modeling and measurements. Our calculated effective carrier lifetime of $CH_3NH_3PbI_3$ agrees with experiments, and is limited by band-to-band radiative recombination and Shockley–Read–Hall defect-assisted non-radiative recombination, whereas the band-to-band non-radiative recombination is found to be negligible. The procedure is further validated by application to the compound semiconductors CdTe and GaAs, and thus can be applied in carrier lifetime simulations in other material systems.

Excited-state carrier dynamics in semiconductors is fundamental to the development of optoelectronic, photovoltaic, photocatalytic and other functional devices working under light illumination[1]. The lifetime of photo-excited non-equilibrium carriers (excess carriers generated by external excitation such as light illumination, which leads to deviation from thermodynamic equilibrium) is an important quantity in determining the performance of these devices. For example, it determines the diffusion length of minority carriers in photovoltaic semiconductors and is thus critical to the efficiency of solar cells. For decades, this important quantity has been obtained mainly through ultrafast time-resolved photoluminescence spectroscopy and transient absorption spectroscopy measurements[2].

Theoretically, conventional first-principles molecular dynamics based on adiabatic approximation does not describe the excited-state carrier dynamics. However, in the past decade, developments in non-adiabatic molecular dynamics (NAMD)[3,4] based on time-dependent density functional theory (TDDFT)[5] have made possible the simulation of excited-state carrier dynamics in semiconductors. A series of breakthroughs have been reported[3,4,6], and first-principles prediction of the carrier lifetime is attracting a great deal of attention. Many recent research works have adopted NAMD simulations based on Erhenfest dynamics or surface hopping schemes to predict the lifetime of non-equilibrium carriers[7–9]. In these studies, non-equilibrium carrier populations were produced by exciting an electron from the occupied electronic state to a higher-energy unoccupied state of the supercell, for example, from the valence band maximum (VBM) to the conduction band minimum (CBM). NAMD simulations were then performed, and the lifetime τ was calculated by fitting the decay of the electron population $\Delta n(t)$ on the excited state to the function $\Delta n(t) \propto \exp(-t/\tau)$, where t is time and 'exp' means the exponential function[7–9]. For example, Qiao and colleagues used NAMD simulation and predicted that the lifetime of photo-excited carriers is 1.5 ns in $CH_3NH_3PbI_3$ (ref. [7]), and similar values have been reported in other studies[8,9]. However, plenty of experiments have reported that the actual lifetime of photo-excited carriers can be as long as several microseconds in $CH_3NH_3PbI_3$ single crystals[10,11]. There is thus a discrepancy between the calculated and experimental values.

To determine the origin of the discrepancy we repeated the NAMD simulation[7]. Our result agreed with theirs, so it appears that no technical error is causing the discrepancy. Kim and Walsh pointed out that non-adiabatic coupling of matrix elements between the valence and conduction bands may be significantly overestimated in NAMD simulations, resulting in exaggerated non-radiative recombination in pristine $CH_3NH_3PbI_3$ and thus leading to the short lifetime[12]. This means that accuracy issues with current NAMD methods may be one possible origin of the discrepancy. On the other hand, as noted in refs. [7] and [13], most NAMD simulations use small supercells. The small supercell size constrains the simulation to have high values for the carrier density and defect density, which can differ from real conditions in experiments. These differences can also cause the observed discrepancy between computation and experiment. If the small-supercell-size effect is the origin, then two open questions need to be answered: (1) what is the physical meaning of the directly calculated carrier lifetime from NAMD simulations and (2) is it possible to use NAMD simulations to calculate a carrier lifetime that can be compared directly to the experimentally measured lifetime of real semiconductors working under light illumination?

In this Brief Communication we started from the fundamental definition of the lifetime of non-equilibrium carriers and developed a systematic procedure for calculating the effective carrier lifetime in real samples based on NAMD simulations, non-radiative

[1]State Key Laboratory of ASIC and System, School of Microelectronics, Fudan University, Shanghai, China. [2]Key Laboratory of Polar Materials and Devices (MOE) and Department of Electronics, East China Normal University, Shanghai, China. [3]Key Laboratory of Computational Physical Sciences (MOE) and Institute of Computational Physical Sciences, Fudan University, Shanghai, China. [4]Department of Physics and ICQD/Hefei National Research Center for Physical Sciences at the Microscale, University of Science and Technology of China, Hefei, Anhui, China. [5]Department of Materials, Imperial College London, London, UK. [6]Shanghai Qi Zhi Institute, Shanghai, China. [7]Beijing Computational Science Research Center, Beijing, China. [8]These authors contributed equally: S. Wang, M. Huang. ✉e-mail: chensy@fudan.edu.cn

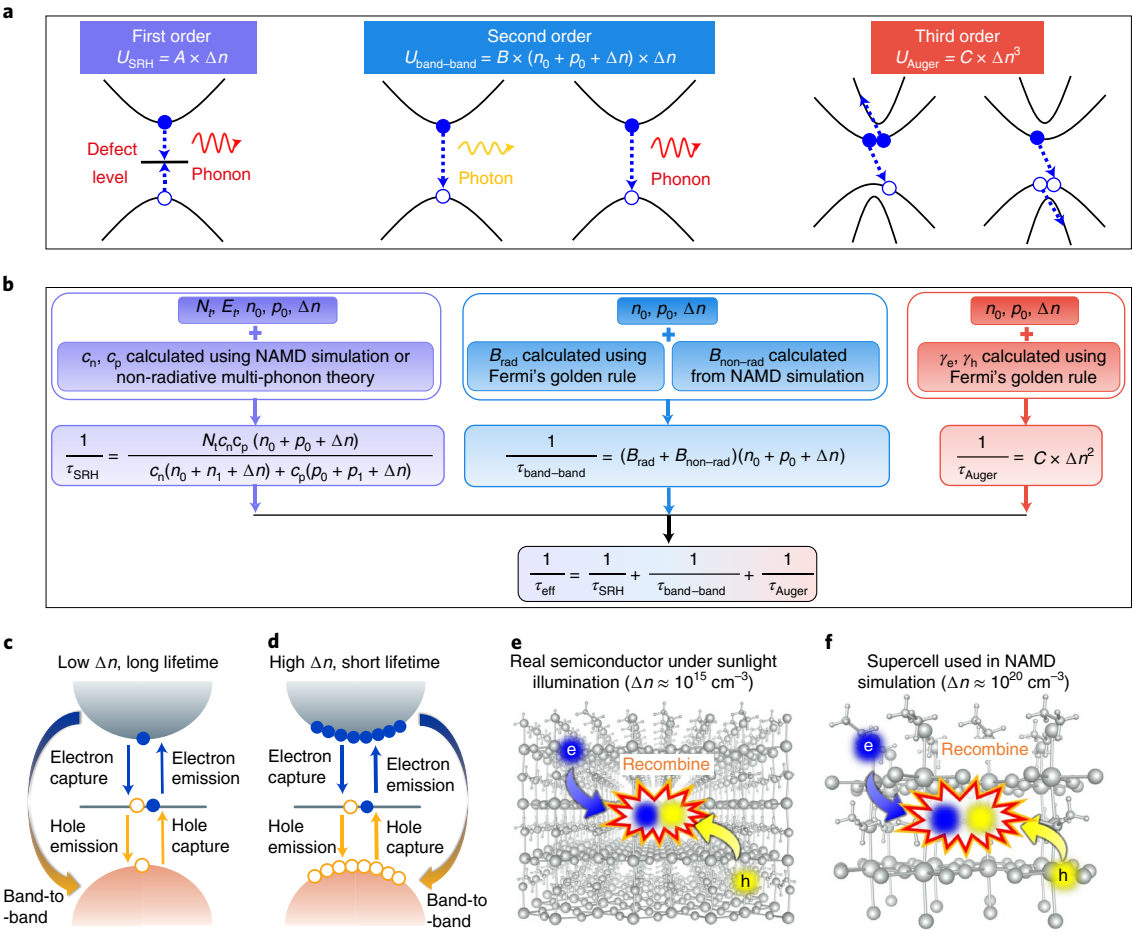

Fig. 1 | Calculating the carrier lifetime for three major recombination mechanisms. a, Schematic plot of first-order defect-assisted SRH, second-order band-to-band radiative or non-radiative, and third-order Auger recombination processes. U represents the recombination rate. A, B and C are SRH, band-to-band and Auger recombination coefficients, respectively. n_0 and p_0 are the densities of electron and hole carriers under the equilibrium condition. Δn is the density of non-equilibrium carriers. **b**, Systematic procedure for calculating the effective lifetime with the three major recombination mechanisms considered. N_t is the density of the recombination-center defects and E_t is the energy of the defect level. n_1 and p_1 are the densities of electron and hole carriers when the Fermi level is located at the defect level. c_n and c_p are the electron and hole capture coefficients of the defect level. B_{rad} and $B_{non\text{-}rad}$ are the band-to-band radiative and non-radiative recombination coefficients. γ_e and γ_h are the e-e-h and h-h-e Auger recombination coefficients. τ_{SRH}, $\tau_{band\text{-}band}$ and τ_{Auger} are the lifetimes for SRH, band-to-band and Auger recombinations, respectively. τ_{eff} is the total effective carrier lifetime when the three recombination mechanisms are all considered. **c**–**f**, Comparison of band-to-band and SRH recombination processes in semiconductors with low and high densities of non-equilibrium carriers: **c** and **d** represent reciprocal band-structure space with electrons (shown by filled blue circles) in the conduction band and holes (open orange circles) in the valence band; **e** and **f** represent the real semiconductor lattice space. The density of non-equilibrium carriers is only ~10^{15} cm^{-3} under sunlight illumination, as shown in **c** and **e**, whereas the density imposed in NAMD simulation supercells can exceed 10^{20} cm^{-3}, as shown in **d** and **f**, which can cause faster electron–hole recombination.

multi-phonon theory and Fermi's golden rule. Using this procedure, we clarified the origins of the discrepancy and determined the dominant recombination mechanisms in $CH_3NH_3PbI_3$ for computing an effective carrier lifetime consistent with experiments. The procedure was further validated on two compound semiconductors, GaAs and CdTe.

In the Methods we derive the procedure and formulae for calculating the effective lifetime τ of non-equilibrium carriers, including the influences of defect-assisted non-radiative Shockley–Read–Hall (SRH; τ_{SRH}), band-to-band radiative ($\tau^{rad}_{band-band}$), band-to-band non-radiative ($\tau^{non-rad}_{band-band}$) and Auger ($\tau_{Auger}$) recombinations. As shown in Fig. 1a, the SRH, band-to-band and Auger recombinations are one-carrier, two-carrier and three-carrier processes, respectively, so their rates have linear, quadratic and cubic dependences on the density of non-equilibrium carriers $\Delta n(0)$ at the $t=0$ moment (when carrier generation stops), meaning that the dominant recombination mechanisms change as $\Delta n(0)$ changes.

Comparing the effective lifetime τ to the directly calculated lifetime from recent NAMD simulations[7,8], we find that recent studies considered only the influences of $\tau^{non-rad}_{band-band}$ and τ_{SRH}. These simulations adopted supercells with several hundreds of atoms, and considered both defect-free supercells and those with defects. For defect-free supercells where no electronic states are found in the bandgap, band-to-band recombination is considered in the simulation, because the recombination occurs between electrons in the CBM and holes in the VBM. The NAMD simulations do not consider any light radiation, so the derived lifetime is the band-to-band non-radiative recombination lifetime, $\tau^{non-rad}_{band-band}$ (Methods). For a supercell with a defect, if a defect level is produced in the bandgap, the defect-assisted SRH and band-to-band non-radiative recombinations are both simulated, and the derived lifetime includes the contributions of τ_{SRH} and $\tau^{non-rad}_{band-band}$. In both cases, the simulated lifetime ($\tau_{band-band}$ and τ_{SRH}) is just a part of the effective lifetime τ, as described by equation (7) in the Methods. If the influences of other

recombination mechanisms (such as $\tau^{rad}_{band-band}$) are more important, incomplete consideration of recombination mechanisms may cause a large difference between the simulated and experimental lifetimes. A detailed comparison for $CH_3NH_3PbI_3$ is shown in the following.

Another origin of the large difference is the dependence of the NAMD-simulated $\tau^{non-rad}_{band-band}$ and τ_{SRH} on $\Delta n(0)$ and N_t (the density of recombination-center defects). In most NAMD simulations, the non-equilibrium electron and hole carriers are generated by exciting an electron from the VBM to the CBM. The supercell usually has several hundred atoms, so the density $\Delta n(0)$ of non-equilibrium carriers is as high as $10^{20}\,cm^{-3}$ (Fig. 1d,f). For example, in a 192-atom $CH_3NH_3PbI_3$ supercell, the density of non-equilibrium carriers is $2.6\times10^{20}\,cm^{-3}$. However, under sunlight illumination (Fig. 1c,e), the excited non-equilibrium carriers have a much lower density, $\sim10^{13}$–$10^{15}\,cm^{-3}$. The imposed $\Delta n(0)$ is therefore much higher than the density in real devices working under sunlight illumination, as compared in Fig. 1c–f. Similarly, the defect density N_t is also seriously overestimated when calculating τ_{SRH}.

Following equation (17) and Supplementary Section 1, $\tau^{non-rad}_{band-band}$ is inversely proportional to $\Delta n(0)$ when $\Delta n(0)$ is high. Following equation (16) and Supplementary Section 2, τ_{SRH} is inversely proportional to N_t. Therefore, the exaggerated $\Delta n(0)$ and N_t imposed in the several-hundred-atom supercells will cause the NAMD-simulated $\tau^{non-rad}_{band-band}$ and τ_{SRH} to be seriously underestimated by orders of magnitude. The lifetime of ~1.5 ns estimated by NAMD simulations is much shorter than the measured lifetime in real samples with smaller values of $\Delta n(0)$ and N_t. In the Methods, we show the formulae to convert the NAMD lifetime to the supercell-size-independent $B_{non\text{-}rad}$ (band-to-band non-radiative recombination coefficient), c_n and c_p (electron and hole capture coefficients). These coefficients can be used to calculate the effective $\tau^{non-rad}_{band-band}$ and τ_{SRH} in real semiconductors with realistic $\Delta n(0)$ and N_t, following the procedure in Fig. 1b. The calculations reveal that the effective $\tau^{non-rad}_{band-band}$ and τ_{SRH} are indeed much longer and do not contradict the experimental lifetime.

Our analysis highlights two origins of the discrepancy between the NAMD-simulated and experimentally measured lifetimes: (1) imposition of high $\Delta n(0)$ and N_t and (2) consideration of only $\tau^{non-rad}_{band-band}$ and τ_{SRH}, while neglecting $\tau^{rad}_{band-band}$, τ_{Auger} and other recombination mechanisms. We now discuss the second point, that is, how the incomplete consideration of recombination mechanisms influences the total effective lifetime τ in $CH_3NH_3PbI_3$ under illumination.

Upon illumination, the non-equilibrium carrier density in $CH_3NH_3PbI_3$ increases and then approaches a steady state, as shown in Fig. 2a. The intensity of light illumination determines the carrier generation rate G. Under sunlight (one-sun) illumination, G is $\sim10^{21}\,cm^{-3}\,s^{-1}$. Under concentrated light, the light intensity becomes stronger, and thus G increases. As G increases, the steady-state carrier density can be increased (as shown in Fig. 2b), so the carrier lifetimes of different recombination mechanisms can be changed. Figure 2d–f shows the calculated $\tau^{non-rad}_{band-band}$, $\tau^{rad}_{band-band}$, τ_{SRH} and τ_{Auger} as functions of G. The details of these calculations are provided in the Methods. τ_{SRH} is inversely proportional to the deep-level recombination-center defect density N_t. However, the defect density in real samples depends on the fabrication conditions and processes. To compare results for $CH_3NH_3PbI_3$ samples fabricated using different processes, Fig. 2d–f presents plots for three representative values of N_t: low at $10^8\,cm^{-3}$, medium at $10^{13}\,cm^{-3}$ and high at $10^{15}\,cm^{-3}$.

Figure 2d shows the lifetime for a low N_t of $10^8\,cm^{-3}$. This low density is possible in $CH_3NH_3PbI_3$ because most of the deep-level defects were reported to have high formation energies and thus low densities under the equilibrium condition[14]. The results showed that τ_{SRH} is always ~0.1 s, which is almost independent of G because the influences of $\Delta n(0)$ on the SRH recombination coefficient A are partially canceled in the numerator and denominator of equation (16). In contrast, $\tau^{rad}_{band-band}$ and $\tau^{non-rad}_{band-band}$ are sensitive to G and decrease quickly as the light intensity and G increase, because $\tau^{rad}_{band-band}$ and $\tau^{non-rad}_{band-band}$ are almost inversely proportional to $\Delta n(0)$ and thus also to G. Comparing τ_{SRH}, $\tau^{rad}_{band-band}$, $\tau^{non-rad}_{band-band}$ and τ_{Auger}, band-to-band radiative recombination is the fastest recombination mechanism and determines the total effective τ when G is lower than $10^{26}\,cm^{-3}\,s^{-1}$, and the Auger recombination dominates at very high G (high carrier densities). In contrast, the SRH and band-to-band non-radiative mechanisms only cause slower recombination and thus just decrease τ slightly according to equations (7) and (20). Under sunlight illumination with G of $\sim10^{21}\,cm^{-3}\,s^{-1}$, the steady-state carrier density is $\sim10^{15}\,cm^{-3}$ when $N_t = 10^8\,cm^{-3}$, and thus the total effective lifetime $\tau \approx \tau^{rad}_{band-band} \approx 1\,\mu s$. For N_t in the range 10^8–$10^{13}\,cm^{-3}$, $\tau^{rad}_{band-band}$ is always shorter than τ_{SRH} and the shortest among the lifetimes of all the recombination mechanisms under sunlight illumination. Therefore, $\tau^{rad}_{band-band}$ always determines the effective lifetime τ to be ~1 μs. The dominance of the band-to-band radiative recombination and the predicted long effective lifetime τ are consistent with the experimental finding of efficient photoluminescence and a measured long carrier lifetime of ~1 μs in $CH_3NH_3PbI_3$ single crystals with $N_t \approx 10^{10}\,cm^{-3}$ (ref. [11]). The consistency between the calculated and measured photoluminescence quantum yield (PLQY) is shown in Fig. 2c and discussed in Supplementary Section 3.

When N_t increases, the dominant recombination mechanism changes. When N_t increases to $10^{13}\,cm^{-3}$, τ_{SRH} and $\tau^{rad}_{band-band}$ are both ~1 μs, as shown in Fig. 2e. The SRH and band-to-band radiative recombination mechanisms are then comparably important. When N_t further increases to $10^{15}\,cm^{-3}$, τ_{SRH} becomes only 10 ns (Fig. 2f). The SRH recombination dominates the total effective lifetime τ when the light intensity is low and G is lower than $10^{25}\,cm^{-3}\,s^{-1}$, while the band-to-band radiative recombination dominates τ only in a small range of G of $\sim10^{26}\,cm^{-3}\,s^{-1}$. For even higher G, Auger recombination dominates. Under sunlight illumination with G of $\sim10^{21}\,cm^{-3}\,s^{-1}$, SRH recombination is dominant. $CH_3NH_3PbI_3$ polycrystals with a high N_t of 10^{15}–$10^{16}\,cm^{-3}$ were reported to have carrier lifetimes in the range 0.01–1 μs (ref. [11]), consistent with the calculated short τ_{SRH} for high N_t.

The above analysis confirms that the lifetime of non-equilibrium carriers in $CH_3NH_3PbI_3$ solar cells should be mainly determined by band-to-band radiative recombination and is usually very long. Only when thin films have a high density of recombination-center defects or dopants can SRH recombination appreciably decrease the lifetime. Across the whole range of G, $\tau^{non-rad}_{band-band}$ is always longer than $\tau^{rad}_{band-band}$ by two orders of magnitude, so the influence of band-to-band non-radiative recombination on the effective τ is negligible in $CH_3NH_3PbI_3$, no matter whether it is under strong or weak light illumination. Therefore, changes in $\tau^{non-rad}_{band-band}$ alone should not be over-interpreted, for example, 1.5 ns for the pristine $CH_3NH_3PbI_3$ compared to 4–11 ns for doped or defective crystals[7]. The experimentally improved performance of $CH_3NH_3PbI_3$ solar cells after the alkaline-metal treatments should result from the substantially increased τ_{SRH}, because the alkaline-metal dopants passivate the recombination-center level of the iodine interstitial and thus give a clean bandgap.

These results demonstrate that it is possible to calculate the carrier lifetime to agree with experimentally measured values, based on NAMD simulations. In Supplementary Section 4 and Extended Data Figs. 1 and 2, we further validate this on two compound semiconductors, CdTe and GaAs, with carrier lifetimes exceeding 1 μs for low defect densities. There are still limitations to the calculation procedure in Fig. 1b: (1) it considers only three major recombination mechanisms and does not consider the surface and interface recombination, which can be important and further shorten the effective carrier lifetime in polycrystalline and thin-film semiconductors;

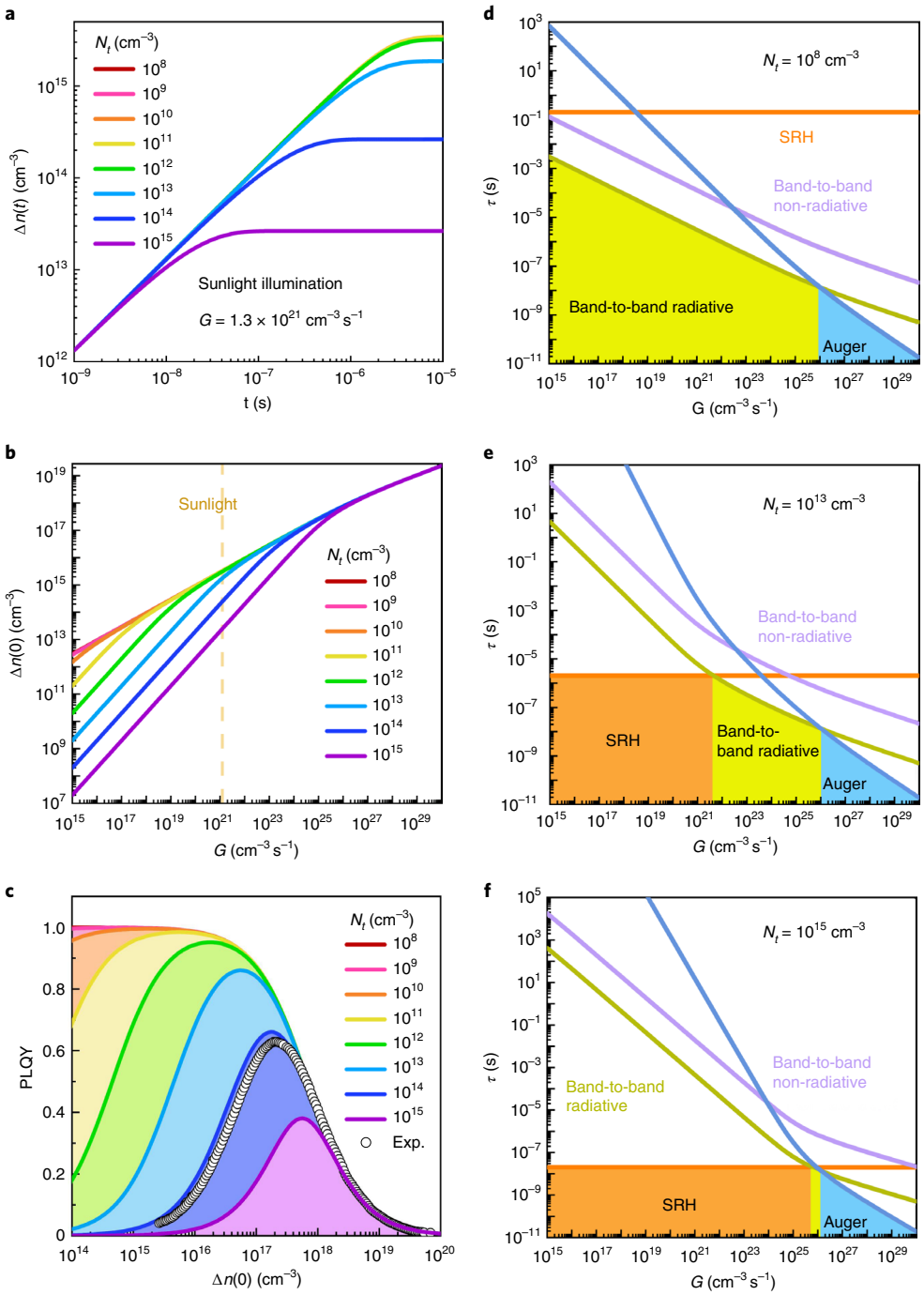

Fig. 2 | Calculated non-equilibrium carrier density, carrier lifetime and PLQY in $CH_3NH_3PbI_3$ under light illumination. a, Time evolution of the non-equilibrium carrier density under sunlight illumination. **b**, Steady-state carrier density as a function of generation rate *G* (light intensity). **c**, PLQY dependence on steady-state carrier density. Experimental data are shown for comparison. **d**–**f**, Carrier lifetime as a function of *G* for $N_t = 10^8$ (**d**), 10^{13} (**e**) and 10^{15} cm^{-3} (**f**). The shaded areas show the ranges of *G* with different dominant recombination mechanisms.

(2) when there are several different types of recombination-center defect in real samples, more than one SRH recombination pathway exist and they should all be considered; (3) the approximations to the exchange-correlation functional in the DFT and the many-body effects can cause errors in the calculated band structure, defect levels, electron–phonon coupling and thus the recombination coefficients, which can also limit the accuracy of the lifetime calculation. These limitations should be noted when comparing the calculated lifetime to the measured value of real samples. Besides carrier recombination, other excited-state carrier-dynamics processes are also widely simulated by NAMD- and TDDFT-related methods, such as the laser-induced phase transition or melting, radiolysis radiation damage, hot carrier cooling and photocurrent generation in a strong external field. The timescales of these processes are attracting great attention. Our finding of the factors influencing the carrier recombination lifetime have implications for the accurate calculations of these timescales. These processes may also have several different mechanisms (or pathways), and their rates may depend on the carrier density and thus on the supercell size used in the simulation. Therefore, the consideration of all relevant

mechanisms and appropriate carrier densities also deserves attention in those studies.

Methods

Definition of carrier lifetime and calculation procedure. As introduced in semiconductor physics textbooks[15], the time derivative of the non-equilibrium carrier density $\Delta n(t)$ is equal to the difference between the generation rate G and the recombination rate U of non-equilibrium carriers:

$$\frac{\mathrm{d}\Delta n\,(t)}{\mathrm{d}t} = G\,(t) - U\,(t). \tag{1}$$

When the generation stops, $G(t)=0$, $\Delta n(t)$ will decay with the rate $-U(t)$. If the recombination rate $U(t)$ depends linearly on $\Delta n(t)$, that is

$$U\,(t) = \frac{\Delta n\,(t)}{\tau}, \tag{2}$$

where τ is a constant,

$$\tau = \frac{\Delta n\,(t)}{U\,(t)}, \tag{3}$$

then the decay of $\Delta n(t)$ will follow

$$\Delta n\,(t) = \Delta n\,(0)\exp\left(-\frac{U\,(t)}{\Delta n\,(t)}t\right) = \Delta n\,(0)\exp\left(-\frac{t}{\tau}\right), \tag{4}$$

where $\Delta n(0)$ is the density of non-equilibrium carriers at the $t=0$ moment when the generation stops. As we can see, in this case, the constant τ means the time when the density decays to $1/e$ of the original value $\Delta n(0)$ after the generation stops, so it is defined as the lifetime of non-equilibrium carriers. Then, equation (1) becomes

$$\frac{\mathrm{d}\Delta n\,(t)}{\mathrm{d}t} = -U\,(t) = -\frac{\Delta n\,(t)}{\tau}. \tag{5}$$

In standard NAMD studies, the lifetime τ is calculated by fitting the decay of the electron population on the excited-state level to the function $\Delta n(t) \propto \exp(-t/\tau)$, which originates from the decay function in equation (4).

According to equation (3), the lifetime τ is determined by the ratio between the density of non-equilibrium carriers $\Delta n(t)$ and the recombination rate $U(t)$. In semiconductors, as shown in Fig. 1a, there are many possible recombination mechanisms, for example, the defect-assisted non-radiative SRH recombination, the band-to-band recombination and the Auger recombination (for polycrystalline thin films, the surface and interface recombination may be important and should also be considered). Therefore, the recombination rate

$$U\,(t) = U_{\mathrm{SRH}}\,(t) + U_{\mathrm{band-band}}\,(t) + U_{\mathrm{Auger}}\,(t) \tag{6}$$

is the sum of the rates of all the mechanisms. Correspondingly, the lifetime that is effective in real semiconductor samples should also be contributed by all the mechanisms:

$$\frac{1}{\tau} = \frac{1}{\tau_{\mathrm{SRH}}} + \frac{1}{\tau_{\mathrm{band-band}}} + \frac{1}{\tau_{\mathrm{Auger}}}, \tag{7}$$

where τ_{SRH}, $\tau_{\mathrm{band\text{–}band}}$ and τ_{Auger} are the lifetimes when only one of the three mechanisms is considered. With this definition, we can also write

$$\tau_{\mathrm{SRH}} = \frac{\Delta n\,(t)}{U_{\mathrm{SRH}}\,(t)}, \tag{8}$$

$$\tau_{\mathrm{band-band}} = \frac{\Delta n\,(t)}{U_{\mathrm{band-band}}\,(t)}, \tag{9}$$

$$\tau_{\mathrm{Auger}} = \frac{\Delta n\,(t)}{U_{\mathrm{Auger}}\,(t)}. \tag{10}$$

As shown by Grundmann[15], the three recombination rates depend not only on $\Delta n(t)$ (for photo-excited non-equilibrium carriers, the densities of non-equilibrium electrons and holes are equal, $\Delta n(t) = \Delta p(t)$), but also on the electron carrier density n_0 and hole carrier density p_0 under the equilibrium state, as described by

$$U_{\mathrm{SRH}}\,(t) = A \times \Delta n\,(t), \tag{11}$$

$$U_{\mathrm{band-band}}\,(t) = B \times [n_0 + p_0 + \Delta n\,(t)] \times \Delta n\,(t), \tag{12}$$

$$U_{\mathrm{Auger}}\,(t) = C \times \Delta n\,(t)^3, \tag{13}$$

in which, A, B and C are the SRH defect-assisted non-radiative, band-to-band and Auger recombination coefficients, respectively, n_0 and p_0 can be calculated as $n_0 = N_{\mathrm{c}}\exp\left(\frac{E_{\mathrm{F}}-E_{\mathrm{CBM}}}{k_0 T}\right)$ and $p_0 = N_{\mathrm{v}}\exp\left(\frac{E_{\mathrm{VBM}}-E_{\mathrm{F}}}{k_0 T}\right)$, where T is the temperature, k_0 is the Boltzmann constant, E_{F} is the Fermi level for $G=0$, E_{VBM} is the VBM level, E_{CBM} is the CBM level, and N_{v} and N_{c} are the effective density of states for valence band and conduction band edges, respectively.

The SRH recombination coefficient A can be calculated following[15]

$$A = \frac{N_t c_{\mathrm{n}} c_{\mathrm{p}}\,(n_0 + p_0 + \Delta n(t))}{c_{\mathrm{n}}\,(n_0 + n_1 + \Delta n(t)) + c_{\mathrm{p}}\,(p_0 + p_1 + \Delta n(t))}, \tag{14}$$

where N_t is the density of the recombination-center defects, c_{n} and c_{p} are the electron capture coefficient and hole capture coefficient of the defect level, respectively, and $n_1 = N_{\mathrm{c}}\exp\left(\frac{E_t-E_{\mathrm{CBM}}}{k_0 T}\right)$ and $p_1 = N_{\mathrm{v}}\exp\left(\frac{E_{\mathrm{VBM}}-E_t}{k_0 T}\right)$, where E_t is the energy of the defect level.

The Auger recombination coefficient C can be calculated following[15]

$$C = \frac{(\gamma_{\mathrm{e}} n_0 + \gamma_{\mathrm{h}} p_0)\,[n_0 + p_0 + \Delta n\,(t)] + (\gamma_{\mathrm{e}} + \gamma_{\mathrm{h}})\,[n_0 + p_0 + \Delta n\,(t)]\,\Delta n\,(t)}{\Delta n\,(t)^2}, \tag{15}$$

in which γ_{e} and γ_{h} are the e-e-h Auger recombination coefficient (one electron at the conduction band is excited to a higher-level state when one electron–hole pair recombines) and the h-h-e Auger recombination coefficient (one hole at the valence band is promoted to a lower-level state when one electron–hole pair recombines).

According to equations (11) to (15), we can notice that the recombination rate $U(t)$ (including $U_{\mathrm{SRH}}(t)$, $U_{\mathrm{band\text{–}band}}(t)$ and $U_{\mathrm{Auger}}(t)$) depends nonlinearly on $\Delta n(t)$, so τ (the carrier lifetime) is not a constant with respect to $\Delta n(t)$. Therefore, in principle, the decay of $\Delta n(t)$ does not follow the simple function in equation (4). When τ was defined as the carrier lifetime (the time when the density decays to $1/e$ of the original value $\Delta n(0)$ after the generation stops) and was calculated by fitting the decay of $\Delta n(t)$ to the function $\exp(-t/\tau)$, we imposed implicitly that τ is a constant and $U(t)$ depends linearly on $\Delta n(t)$ in the following recombination processes after the generation stops. Of course, the fitting cannot be good if τ has a strong dependence on $\Delta n(t)$. Therefore, when we discuss the carrier lifetime τ, we must pay attention to this dependence and note that τ can be approximated as a constant only for a small range of t in which $\Delta n(t)$ does not change significantly. In such a small range of t, $\Delta n(t)$ can be approximated as $\Delta n(0)$, which is the value at the moment when the generation stops. With $\Delta n(0)$, the recombination coefficients A and C can thus be determined, then the corresponding lifetime can be calculated as

$$\tau_{\mathrm{SRH}} = \frac{c_{\mathrm{n}}\,(n_0 + n_1 + \Delta n(0)) + c_{\mathrm{p}}\,(p_0 + p_1 + \Delta n(0))}{N_t c_{\mathrm{n}} c_{\mathrm{p}}\,(n_0 + p_0 + \Delta n(0))} \tag{16}$$

$$\tau_{\mathrm{band-band}} = \frac{1}{B \times [n_0 + p_0 + \Delta n\,(0)]} \tag{17}$$

$$\tau_{\mathrm{Auger}} = \frac{1}{(\gamma_{\mathrm{e}} n_0 + \gamma_{\mathrm{h}} p_0)\,[n_0 + p_0 + \Delta n\,(0)] + (\gamma_{\mathrm{e}} + \gamma_{\mathrm{h}})\,[n_0 + p_0 + \Delta n\,(0)]\,\Delta n\,(0)}. \tag{18}$$

In devices operating under continuous-light illumination, the density of non-equilibrium carriers should reach a steady state after the generation and recombination are counterbalanced, then the steady-state density should be considered as $\Delta n(0)$ when calculating the carrier lifetime according to equations (16), (17) and (18), as shown in Fig. 2a for the steady-state density in $CH_3NH_3PbI_3$ under light illumination.

As shown in Fig. 1a, defect-assisted SRH non-radiative recombination occurs between one carrier (electron or hole) and one defect, so the dependence of U_{SRH} on Δn (abbreviation of $\Delta n(0)$) is approximately first order in equation (11). The band-to-band recombination occurs between two carriers (one electron and one hole), so the dependence of $U_{\mathrm{band\text{–}band}}$ on Δn is approximately second order in equation (12). Auger recombination occurs between three carriers (two electrons and one hole, or one electron and two holes), so the dependence of U_{Auger} on Δn is approximately third order in equation (13). Therefore, when the density Δn of photo-excited non-equilibrium carriers is small, U_{SRH} and $U_{\mathrm{band\text{–}band}}$ are much larger than U_{Auger} and so τ_{SRH} and $\tau_{\mathrm{band\text{–}band}}$ determine τ; but when Δn is large, U_{SRH} and $U_{\mathrm{band\text{–}band}}$ are much smaller than U_{Auger} so τ_{Auger} determines τ (ref. [16]).

To calculate the total effective lifetime τ of non-equilibrium carriers in real semiconductor samples with a certain defect density N_t, equilibrium carrier density n_0 (p_0) and non-equilibrium carrier density $\Delta n(0)$, τ_{SRH}, $\tau_{\mathrm{band\text{–}band}}$ and τ_{Auger} should all be calculated and combined. A procedure is plotted in Fig. 1b to show the flow of the calculations, which include the following:

(1) For a given type of defect with energy level E_t, calculate its electron and hole capture coefficients, c_{n} and c_{p}. These can be calculated from the NAMD simulation or by using non-radiative multi-phonon (NMP) theory[17,18], as discussed

in the section 'Calculation of defect-assisted SRH recombination lifetime'. With E_t, c_n and c_p, τ_{SRH} can be calculated for any given N_t, n_0 (p_0) and $\Delta n(0)$.

(2) Calculate the band-to-band recombination coefficient B. Details of the methods for this are discussed in the section 'Calculation of band-to-band recombination lifetime'. With B, $\tau_{band-band}$ can be calculated for any given n_0 (p_0) and $\Delta n(0)$.

(3) Calculate the Auger recombination coefficients γ_e and γ_h. The methods for this are discussed in the section 'Calculation of Auger recombination lifetime'. With γ_e and γ_h, τ_{Auger} can be calculated for any given n_0 (p_0) and $\Delta n(0)$.

After the calculation of τ_{SRH}, $\tau_{band-band}$ and τ_{Auger}, the effective lifetime τ can be derived according to equation (7) and the value can be compared directly with the experimentally measured lifetime in real samples with given N_t, n_0 (p_0) and $\Delta n(0)$.

Calculation of band-to-band recombination lifetime. As shown in Fig. 1a, there are two types of band-to-band recombination: radiative and non-radiative. For band-to-band radiative recombination, the energy of non-equilibrium carriers is converted into the energy of an emitted photon. For band-to-band non-radiative recombination, the energy of non-equilibrium carriers is converted into the energy of the vibration energy of ions through electron–phonon coupling. The recombination rate and lifetime are contributed by both types, as described by

$$\begin{aligned} U_{band-band}(t) &= U^{rad}_{band-band}(t) + U^{non-rad}_{band-band}(t) \\ &= \left(B_{rad} + B_{non-rad}\right) \times [n_0 + p_0 + \Delta n(t)] \times \Delta n(t) \end{aligned} \tag{19}$$

$$\frac{1}{\tau_{band-band}} = \frac{1}{\tau^{rad}_{band-band}} + \frac{1}{\tau^{non-rad}_{band-band}}. \tag{20}$$

Correspondingly, the recombination coefficient B is also contributed by two parts, B_{rad} and $B_{non-rad}$.

In the standard textbook description, band-to-band recombination is considered a radiative process[19], whereas the non-radiative rate is expected to be low under normal operation conditions. In the following, we will show the calculation methods for B_{rad} and $B_{non-rad}$.

Band-to-band radiative recombination coefficient B_{rad}. The band-to-band radiative recombination coefficient B_{rad} can be calculated using Fermi's golden rule and the transition dipole moment (momentum matrix elements)[19,20] according to

$$B_{rad} = \frac{n_r e^2}{3\pi\varepsilon_0 m_e^2 c^3 \hbar^2 n^2 V} \sum\nolimits_{cvk} f_{ck}(1 - f_{vk})(E_{ck} - E_{vk})\left(p_x^2 + p_y^2 + p_z^2\right), \tag{21}$$

where n_r is the refractive index of the material, e is the elementary charge, ε_0 is the vacuum permittivity, m_e is the mass of a free electron, c is the speed of light, n is the non-equilibrium carrier density, V is the volume of the cell used for the calculation, and p_x, p_y, p_z are the momentum matrix elements along the x, y, z directions between conduction band c and valence band v at momentum point k. f_{ck} and f_{vk} are the Fermi–Dirac occupation factors, which are related to the electron and hole quasi-Fermi levels E_{Fn} and E_{Fp} with the carrier density n:

$$f_{ck} = \frac{1}{1 + e^{\frac{E_{ck} - E_{Fn}}{k_B T}}} \tag{22}$$

$$f_{vk} = \frac{1}{1 + e^{\frac{E_{vk} - E_{Fp}}{k_B T}}}. \tag{23}$$

To obtain the quasi-Fermi level with a given carrier density n, one must perform a first-principles calculation with a very dense k-point mesh so that the effective density of states can be accurately depicted by the eigenvalues calculated at those k-points. The summation of the Fermi–Dirac occupation of electrons and holes should be equal to the number of carriers within the volume V:

$$\sum\nolimits_{ck} f_{ck} = \sum\nolimits_{vk}(1 - f_{vk}) = nVN_k. \tag{24}$$

By self-consistently solving the above equation, we can obtain the quasi-Fermi levels for electrons and holes, respectively.

In reality, calculating the momentum matrix elements on a very dense k-point mesh using a hybrid functional can be difficult due to the computational cost. Alternatively, we can adopt a mixed scheme. Taking zinc-blende GaAs as an example, a 15×15×15 mesh is used for a small region near the Γ point ($|k_i| \le 0.1 \times 2\pi/a$, where $i = x, y, z$ and a is the lattice constant), which corresponds to a 75×75×75 mesh for the whole Brillouin zone (BZ) sampling. For the rest of the BZ, we use a 15×15×15 mesh. Because the k-point mesh is much denser within the range of $|k_i| \le 0.1 \times 2\pi/a$, the weight of those k-points should be rescaled. By summing over all the k-points, we can obtain coefficient B_{rad} at carrier density n. The many-body effects of carriers may influence the calculated B_{rad} (ref. [21]), so it should be taken into consideration for the very accurate calculation of B_{rad}.

In Supplementary Section 5 we show our calculated values of B_{rad} for $CH_3NH_3PbI_3$, GaAs and CdTe, which are consistent with those calculated by other groups[20]. When the carrier density is less than 10^{18} cm^{-3}, B_{rad} is almost constant, and when the carrier density is higher than 10^{18} cm^{-3}, the system starts to enter the degenerate region and B_{rad} starts to drop. In the semiconductors under sunlight illumination, the carrier density is much lower than 10^{18} cm^{-3}, as shown in Fig. 2b, so the variation in B_{rad} is neglected.

Band-to-band non-radiative recombination $B_{non-rad}$. In recent NAMD simulations[7–9] of band-to-band recombination, carrier excitation is modeled through a change in the occupation numbers of the valence and conduction bands of the defect-free supercell. Recombination towards the ground state is then simulated by NAMD, and the band-to-band recombination lifetime τ is calculated by fitting the decay of the electron population using $\Delta n(t) \propto \exp(-t/\tau)$. These simulations are in the microcanonical (NVE) ensemble, so the electronic energy decrease is converted into vibrational (kinetic) energy through electron–phonon coupling, which obeys the energy conservation rule. Emission of light is not considered, so the NAMD-simulated band-to-band recombination is non-radiative and the associated lifetime is, in fact, $\tau^{non-rad}_{band-band}$. This was also pointed out by Kim and Walsh[12].

Here we give an introduction to the calculation procedure for calculating $\tau^{non-rad}_{band-band}$ in the defect-free semiconductor (taking $CH_3NH_3PbI_3$ as an example) supercell using the NAMD method as implemented in the PYthon eXtension for Ab Initio Dynamics (PYXAID) code. We use the decoherence-induced surface hopping (DISH) approach to account for the decoherence effect, which is required in the simulation of the recombination process across significant energy gaps. Before the NAMD simulation using PYXAID, we first perform Born–Oppenheimer molecular dynamics (BOMD) and electronic structure calculations using the DFT and planewave pseudopotential methods as implemented in the Vienna ab initio package (VASP) code. Starting from the optimized geometry of a 192-atom supercell at 0 K, the system is heated to 300 K using the velocity rescaling method for 2 ps. Then, 4-ps BOMD trajectories with a 1-fs timestep are generated in the microcanonical ensemble. All the geometries are used to calculate the non-adiabatic couplings (NAC) at the direct-bandgap Γ point using PYXAID. To simulate the charge carrier recombination processes, the 4-ps non-adiabatic Hamiltonians are iterated multiple times. Four hundred initial conditions are chosen randomly from the 4-ps trajectory to sample the canonical distribution of the atomic coordinates. After that, 2,000 realizations are performed to sample the real-time population. To simulate the band-to-band non-radiative recombination in the defect-free supercell, the electron is excited directly from the VBM to the CBM, then the calculated time evolution of the excited-state population is fitted to the exponential function $\Delta n(t) \propto \exp(-t/\tau)$ (it can be approximated by a linear function $\Delta n(t) \propto 1 - t/\tau$) in a short timescale, which gives a lifetime τ.

Because the $\Delta n(0)$ imposed in the NAMD supercell simulations is very high (~10^{20} cm^{-3}), much higher than the typical values (~10^{15} cm^{-3}) in semiconductors under sunlight illumination (as compared in Fig. 1), the directly calculated lifetime from NAMD simulations should be seriously underestimated and very short, ~1 ns, as demonstrated in Supplementary Fig. 1c for $\Delta n(0)$ of ~10^{20} cm^{-3}. If, instead, the simulation uses a very large supercell with 10^7 atoms, $\Delta n(0)$ decreases to ~10^{15} cm^{-3}, and $\tau^{non-rad}_{band-band}$ can be as long as 10^5 ns, as demonstrated in Supplementary Fig. 1d. Based on the analysis, the short lifetime of 1.5 ns derived from NAMD simulations is not the effective $\tau^{non-rad}_{band-band}$ or the total effective τ in real samples, so it is meaningless to directly compare the value to the experimental lifetime.

A suitable way to predict the effective $\tau^{non-rad}_{band-band}$ is by adopting equation (17) to derive the supercell-size-independent recombination coefficient $B_{non-rad}$ from the raw $\tau^{non-rad}_{band-band}$ derived from the NAMD supercell simulations. Equation (17) is changed to

$$B_{non-rad} = \frac{1}{\tau^{non-rad}_{band-band} \times [n_0 + p_0 + \Delta n(0)]}. \tag{25}$$

The densities of the equilibrium carriers, n_0 and p_0, should be small in the defect-free (dopant-free) supercell and can be neglected compared to $\Delta n(0)$, because the bandgap is above 1.5 eV and the thermal excitation of carriers can be neglected. As a result, $B_{non-rad} = \frac{1}{\tau^{non-rad}_{band-band} \times \Delta n(0)}$. With $B_{non-rad}$, the effective $\tau^{non-rad}_{band-band}$ for low $\Delta n(0)$ in real samples can be calculated according to equation (17). Using this conversion procedure, we revisited the NAMD-simulated $\tau^{non-rad}_{band-band}$ for 11 different semiconductors and found more longer effective $\tau^{non-rad}_{band-band}$ values, as discussed in Supplementary Section 6.

Calculation of defect-assisted SRH recombination lifetime. According to equation (16), τ_{SRH} can be calculated if the electron capture coefficient c_n and hole capture coefficient c_p of the defect level are known. c_n and c_p can be calculated using the NAMD simulation or NMP theory[17,18].

The NAMD calculation procedure for c_n and c_p is similar to that for $B_{non-rad}$. The difference is that there is a recombination-center defect in the supercell

that produces a deep level in the bandgap, so the many-electron state basis sets of the NAMD simulation include the VBM, CBM and defect-level states. After an electron is excited from the VBM level to the CBM level, there are different transitions including those from the CBM to the defect level (the excited state to the intermediate defect-trap state in the many-electron state picture), the defect level to the VBM (the defect-trap state to the ground state) and from the CBM to the VBM (the excited state to the ground state). Their transition rates can be determined from the short-time DISH-based NAMD simulations, then the rates can be used to solve the defect-assisted coupled kinetic equations of electron–hole recombination in a nanosecond timescale. The calculated time evolution of the defect-trap state population can then be used to calculate the electron trapping time τ_e and hole trapping time τ_h of the defect level by exponential fitting, as described by Shi and colleagues[22].

Equation (16) and Supplementary Section 2 show the inversely proportional dependence of τ_{SRH} (similarly for electron and hole trapping times τ_e and τ_h) on N_t, so the derived lifetime from the NAMD simulations[22] with one defect in a several-hundred-atom supercell ($N_t \approx 10^{20}\,cm^{-3}$) should not be interpreted as the effective τ_{SRH} (similarly for τ_e and τ_h) either. The lifetime fitted from the small-supercell NAMD simulations should be converted to the N_t-independent electron capture coefficient c_n and hole capture coefficient c_p of the defect according to equation (16), then the effective τ_{SRH} in real samples with reasonable N_t can be calculated using the same equation. Because n_0, p_0, n_1 and p_1 in equation (16) are all small for deep-level defects, but $\Delta n(0)$ is very large in the NAMD simulation supercell, $\tau_e = \frac{1}{N_t c_n}$ for electron capture and $\tau_h = \frac{1}{N_t c_p}$ for hole capture. For example, Shi and colleagues performed NAMD simulations of the charge-trapping processes in $CH_3NH_3PbBr_3$ containing the DY^- center[22]. The obtained decay time, τ_e, is 1.9 ns for CBM-to-defect trapping and τ_h is 4.7×10^{-2} ns for VBM-to-defect trapping. With the defect density ($1.8\times10^{20}\,cm^{-3}$) in their NAMD simulation, we can extract $c_n = 2.9\times10^{-12}\,cm^3\,s^{-1}$ and $c_p = 1.2\times10^{-10}\,cm^3\,s^{-1}$. The values are low compared to the normal carrier capture coefficients of defects in semiconductors ($10^{-7}\,cm^3\,s^{-1}$)[17]. Assuming that N_t in real semiconductors is $10^{15}\,cm^{-3}$ and $\Delta n(0) = 10^{15}\,cm^{-3}$, $\tau_{SRH} = 345\,\mu s$ according to equation (16). Therefore, according to the NAMD simulation, such a defect should not cause serious limit to the lifetime of photo-excited carriers in $MAPbBr_3$ when the densities of the defect and photo-excited carriers are at a medium level.

As well as using the NAMD simulation, c_n and c_p can also be calculated using NMP theory based on the static coupling approximation derived from Fermi's golden rule[17,18]:

$$c_n = Vf\frac{2\pi}{\hbar}g\sum_k \left|\left\langle \psi_i \left| \frac{\partial H}{\partial Q_k} \right| \psi_f \right\rangle\right|^2 \sum_m p_m \sum_n |\langle \chi_{im}|Q_k - Q_{k0}|\chi_{fn}\rangle|^2 \delta(\Delta E + E_{im} - E_{fn}), \quad (26)$$

where V is the supercell volume, f is the Sommerfeld factor representing the Coulomb interaction between the charged defect and free carriers, $\hbar$ is the reduced Planck constant, g is the degeneracy factor, $\left\langle \psi_i \left| \frac{\partial H}{\partial Q_k} \right| \psi_f \right\rangle$ is the electron–phonon coupling matrix element along phonon mode k, p_m is the Boltzmann occupation factor of the initial vibrational state m of phonon mode k, χ_{im} and χ_{fn} are the initial and final vibrational wavefunctions, and E_{im} and E_{fn} are their eigenvalues. Q_{k0} refers to the geometry where the Hamiltonian H is expanded. By summing these quantities over all phonon modes using an infinite-integral scheme, one can obtain the carrier capture coefficient. Alternatively, adopting a single-phonon approximation simplifies the formula, and one can numerically calculate the integrals instead. A series of algorithms and codes have been developed for such calculations during the past decade[17,18].

When calculating coefficients c_n and c_p using either NAMD simulation or NMP theory, the convergence of the coefficients with respect to the supercell size should be tested, because the electron–phonon coupling effect for defects with different electronic states and phonon modes (localized or delocalized) can be quite different, and may not be accurately described by small supercells[4].

Calculation of Auger recombination lifetime. Equation (18) shows that τ_{Auger} can be calculated when the e-e-h recombination coefficient γ_e and h-h-e coefficient γ_h are known. For direct Auger recombination, γ_e (similarly for γ_h) can be calculated based on time-dependent perturbation theory using Fermi's golden rule[23]:

$$\gamma_e = \frac{2\pi}{\hbar n^3}\sum_{1234} f_1 f_2 (1-f_3)(1-f_4)|M_{1234}|^2 \delta(E_1 + E_2 - E_3 - E_4) \quad (27)$$

where 1 and 2 indicate the single-particle states of electrons, and 3 and 4 those of holes. f_1, f_2, f_3 and f_4 are the Fermi–Dirac occupation factors of these states depending on the quasi-Fermi levels for electrons and holes, which can be calculated in the same way as described in the calculation methods for B_{rad}. M_{1234} is the screened Auger matrix element, which can be calculated from the single-particle wavefunctions

$$M_{1234} = \langle \psi_1\psi_2 | W | \psi_3\psi_4\rangle - \langle \psi_1\psi_2 | W | \psi_4\psi_3\rangle \quad (28)$$

where W is the screened Coulomb operator, $\langle \psi_1\psi_2 | W | \psi_3\psi_4\rangle$ is the direct Coulomb term, and $\langle \psi_1\psi_2 | W | \psi_4\psi_3\rangle$ is the exchange term.

An open-source code that implements this calculation method of the Auger recombination coefficients using the brute-force algorithm is available[23]. The calculated γ_e and γ_h are 2.7×10^{-29}, $4.6\times10^{-29}\,cm^6\,s^{-1}$ for $CH_3NH_3PbI_3$ (ref. [23]).

Calculation of effective lifetime under light illumination. The effective lifetime τ of non-equilibrium carriers is influenced by all recombination mechanisms. τ_{SRH}, $\tau^{non-rad}_{band-band}$, $\tau^{rad}_{band-band}$ and τ_{Auger} depend on the density of non-equilibrium carriers $\Delta n(0)$, the density of equilibrium carriers n_0 and p_0, and the density of recombination-center defects N_t. When calculating τ, these quantities should be obtained as summarized by the calculation procedure in Fig. 1b. For a semiconductor sample, the density (N_t) of recombination-center defect or dopant and the density of the equilibrium carriers (n_0 and p_0) are fixed for a certain fabrication condition and process (n_0 and p_0 can be determined if N_t is known). With the densities and energy levels of all shallow or deep defects and dopants, n_0 and p_0 can be calculated based on the charge-neutrality condition. For example, $n_0 = p_0 = 0.85\times10^6\,cm^{-3}$ for undoped $CH_3NH_3PbI_3$. However, the density of non-equilibrium carriers $\Delta n(0)$ in the real samples depends on the working environment, for example, the intensity of the light illumination. To calculate the total effective lifetime τ, for example, in $CH_3NH_3PbI_3$, we will first show how to calculate $\Delta n(0)$ under illumination.

In the dark, the density of non-equilibrium carriers is 0. If the above-bandgap illumination starts at $t = 0$, the density $\Delta n(t)$ increases with the rate $\frac{d\Delta n(t)}{dt}$ given by equation (1). After a certain time, the system will reach a steady state because the carrier generation and recombination are balanced, and the carrier density $\Delta n(t)$ will maintain at a steady value, as given by

$$\frac{d\Delta n(t)}{dt} = G(t) - U(t) = 0. \quad (29)$$

In Fig. 2a we simulate the increasing process of $\Delta n(t)$ in the $CH_3NH_3PbI_3$ thin film. For sunlight (one-sun) illumination on thin films with layer thickness d, the generation rate $G(t)$ of non-equilibrium carriers is a constant and can be calculated as

$$G(t) = (hc)^{-1}\int f_{solar}(\lambda)\,\alpha(\lambda)\exp(-\alpha(\lambda)\,d)\,\lambda d\lambda \quad (30)$$

where d is the film thickness of the absorption layer, h is the Planck constant, c is the speed of light, $f_{solar}(\lambda)$ is the ASTM G173-03 Global Tilt reference spectrum for the solar spectral irradiance distribution, $\alpha(\lambda)$ is the absorbance spectrum of the semiconductor and λ is the wavelength of the light. The calculated G is $1.3\times10^{21}\,cm^{-3}\,s^{-1}$ for the 300-nm-thick film. The recombination rate $U(t)$ can be calculated using

$$U = U_{SRH} + U_{band-band} + U_{Auger} = A\times\Delta n(t) + (B_{rad} + B_{non-rad})\times[n_0 + p_0 + \Delta n(t)]\times\Delta n(t) + C\times\Delta n(t)^3, \quad (31)$$

in which the SRH, band-to-band (radiative and non-radiative) and Auger recombinations are all considered. The SRH recombination coefficient A is calculated assuming the density of the recombination-center defect has a series of representative values in the range $N_t = 10^8$–$10^{15}\,cm^{-3}$ (to represent different samples with only shallow defects, a medium density of deep defects and a high density of deep defects), electron capture coefficient and hole capture coefficients of $c_n = c_p = 10^{-7}\,cm^3\,s^{-1}$ (normal carrier capture coefficients of defects in semiconductors[17]) and $n_0 = p_0 = 0.85\times10^6\,cm^{-3}$. The band-to-band radiative recombination coefficient $B_{rad} = 1.1\times10^{-10}\,cm^3\,s^{-1}$ in $CH_3NH_3PbI_3$ was calculated by Zhang and colleagues[20], and is close to our calculated value in Supplementary Section 5. The band-to-band non-radiative recombination coefficient $B_{non-rad} = 2.6\times10^{-12}\,cm^3\,s^{-1}$ was derived based on the NAMD simulation of Qiao and colleagues[7]. The Auger recombination coefficients[23] are $\gamma_e = 2.7\times10^{-29}$ and $\gamma_h = 4.6\times10^{-29}\,cm^6\,s^{-1}$. All these quantities can be calculated using the methods shown above and standard DFT calculations for any crystalline semiconductors.

With G and U, $\Delta n(t)$ as a function of t can be simulated, as shown in Fig. 2a. At $t = 0$, $\Delta n(t)$ is 0, then it starts to increase under the light illumination. As t increases, the system finally reaches the steady state and $\Delta n(t)$ plateaus. As shown in Fig. 2a, $\Delta n(t)$ reaches a steady value of $2.7\times10^{13}\,cm^{-3}$ at $t \approx 10^{-7}$ s when $N_t = 10^{15}\,cm^{-3}$, whereas it reaches a steady value of $3.4\times10^{15}\,cm^{-3}$ at $t \approx 10^{-5}$ s for $N_t = 10^8\,cm^{-3}$. Therefore, the steady density of non-equilibrium carriers and the time taken to reach the steady state are sensitive to the defect density. A higher defect density facilitates SRH recombination and thus decreases the time to reach the steady state.

In Fig. 2b we calculated the steady density of non-equilibrium carriers for various G, corresponding to different illumination intensities. When G is below $10^{26}\,cm^{-3}\,s^{-1}$, the steady-state density increases almost linearly as G increases. The generation rate under sunlight illumination is shown by the dashed line, and the steady density is ~$10^{13}\,cm^{-3}$ for $N_t = 10^{15}\,cm^{-3}$ and $10^{15}\,cm^{-3}$ for $N_t = 10^8\,cm^{-3}$, much lower than the imposed density of non-equilibrium carriers (~$10^{20}\,cm^{-3}$) in small NAMD-simulation supercells.

The steady density of non-equilibrium carriers under sunlight illumination should be taken as $\Delta n(0)$ when calculating the lifetime of non-equilibrium carriers in $CH_3NH_3PbI_3$ thin-film solar cells. Because the steady-state density changes with G, the lifetime should also change with G. When $\Delta n(0)$, N_t, E_t, c_n, c_p, n_0, p_0, B_{rad} and $B_{non\text{-}rad}$, γ_e and γ_h are known, τ_{SRH}, $\tau^{rad}_{band-band}$, $\tau^{non-rad}_{band-band}$ and τ_{Auger} can be calculated directly, following the procedure in Fig. 1b. Figure 2d–f show how G influences the calculated τ_{SRH}, $\tau^{rad}_{band-band}$, $\tau^{non-rad}_{band-band}$ and τ_{Auger} of $CH_3NH_3PbI_3$. In Supplementary Section 4, we further demonstrate the calculation of effective carrier lifetimes in GaAs and CdTe with different carrier generation rates and different defect densities.

With the recombination rates of different mechanisms in equation (31), we can also calculate the internal PLQY:

$$\eta = \frac{U^{rad}_{band-band}}{U_{SRH}+U^{rad}_{band-band}+U^{non-rad}_{band-band}+U_{Auger}} = \frac{B_{rad}\times[n_0+p_0+\Delta n(0)]}{A+(B_{rad}+B_{non-rad})\times[n_0+p_0+\Delta n(0)]+C\times\Delta n(0)^2}, \quad (32)$$

because only band-to-band radiative recombination is a radiative process, whereas the SRH, band-to-band non-radiative and Auger recombinations are non-radiative. The calculated PLQY results are discussed in Supplementary Section 3.

Data availability

The raw data for the first-principles calculations have been deposited in the Zenodo repository[24], including molecular dynamics calculations, non-adiabatic coupling calculations and momentum matrix elements calculations. Source data are provided with this Paper. Those data are generated by the code developed for this study.

Code availability

The effective carrier lifetime (ECL) code is published in the Code Ocean repository[25].

Received: 16 February 2022; Accepted: 11 July 2022;
Published online: 22 August 2022

References

1. Feldmann, S. et al. Photodoping through local charge carrier accumulation in alloyed hybrid perovskites for highly efficient luminescence. *Nat. Photon.* **14**, 123–128 (2020).
2. Guo, Z. et al. Long-range hot-carrier transport in hybrid perovskites visualized by ultrafast microscopy. *Science* **356**, 59–62 (2017).
3. Crespo-Otero, R. & Barbatti, M. Recent advances and perspectives on nonadiabatic mixed quantum-classical dynamics. *Chem. Rev.* **118**, 7026–7068 (2018).
4. Chu, W., Zheng, Q., Prezhdo Oleg, V., Zhao, J. & Saidi Wissam, A. Low-frequency lattice phonons in halide perovskites explain high defect tolerance toward electron-hole recombination. *Sci. Adv.* **6**, eaaw7453 (2020).
5. Runge, E. & Gross, E. K. U. Density-functional theory for time-dependent systems. *Phys. Rev. Lett.* **52**, 997–1000 (1984).
6. Pan, J. Computationally probing exciton dynamics. *Nat. Comput. Sci.* **1**, 246 (2021).
7. Qiao, L., Fang, W.-H., Long, R. & Prezhdo, O. V. Extending carrier lifetimes in lead halide perovskites with alkali metals by passivating and eliminating halide interstitial defects. *Angew. Chem. Int. Ed.* **59**, 4684–4690 (2020).
8. He, J., Fang, W.-H., Long, R. & Prezhdo, O. V. Increased lattice stiffness suppresses nonradiative charge recombination in $MAPbI_3$ doped with larger cations: time-domain Ab initio analysis. *ACS Energy Lett.* **3**, 2070–2076 (2018).
9. Huang, Y. et al. A-site cation engineering for highly efficient $MAPbI_3$ single-crystal X-ray detector. *Angew. Chem. Int. Ed.* **58**, 17834–17842 (2019).
10. deQuilettes, D. W. et al. Photoluminescence lifetimes exceeding 8 μs and quantum yields exceeding 30% in hybrid perovskite thin films by ligand passivation. *ACS Energy Lett.* **1**, 438–444 (2016).
11. Brenner, T. M., Egger, D. A., Kronik, L., Hodes, G. & Cahen, D. Hybrid organic–inorganic perovskites: low-cost semiconductors with intriguing charge-transport properties. *Nat. Rev. Mater.* **1**, 15007 (2016).
12. Kim, S. & Walsh, A. Comment on 'Low-frequency lattice phonons in halide perovskites explain high defect tolerance toward electron-hole recombination'. Preprint at https://arxiv.org/abs2003.05394 (2020).
13. Chu, W., Zheng, Q., Prezhdo, O. V., Zhao, J. & Saidi, W. A. Response to comment on 'Low-frequency lattice phonons in halide perovskites explain high defect tolerance toward electron-hole recombination'. Preprint at https://arxiv.org/abs/2004.12559 (2020).
14. Yin, W.-J., Shi, T. & Yan, Y. Unusual defect physics in $CH_3NH_3PbI_3$ perovskite solar cell absorber. *Appl. Phys. Lett.* **104**, 063903 (2014).
15. Grundmann, M. *Physics of Semiconductors* Vol. 11 (Springer, 2010).
16. Zhang, X., Shen, J.-X. & Van de Walle, C. G. First-principles simulation of carrier recombination mechanisms in halide perovskites. *Adv. Energy Mater.* **10**, 1902830 (2020).
17. Alkauskas, A., Yan, Q. & Van de Walle, C. G. First-principles theory of nonradiative carrier capture via multiphonon emission. *Phys. Rev. B* **90**, 075202 (2014).
18. Shi, L., Xu, K. & Wang, L.-W. Comparative study of ab initio nonradiative recombination rate calculations under different formalisms. *Phys. Rev. B* **91**, 205315 (2015).
19. Landsberg, P. T. *Recombination in Semiconductors* (Cambridge Univ. Press, 2003).
20. Zhang, X., Shen, J.-X., Wang, W. & Van de Walle, C. G. First-principles analysis of radiative recombination in lead-halide perovskites. *ACS Energy Lett.* **3**, 2329–2334 (2018).
21. Davies, C. L. et al. Bimolecular recombination in methylammonium lead triiodide perovskite is an inverse absorption process. *Nat. Commun.* **9**, 293 (2018).
22. Shi, R., Fang, W.-H., Vasenko, A. S., Long, R. & Prezhdo, O. V. Efficient passivation of DY center in $CH_3NH_3PbBr_3$ by chlorine: quantum molecular dynamics. *Nano Res.* **15**, 2112–2122 (2022).
23. Shen, J.-X., Zhang, X., Das, S., Kioupakis, E. & Van de Walle, C. G. Unexpectedly strong Auger recombination in halide perovskites. *Adv. Energy Mater.* **8**, 1801027 (2018).
24. Wang, S., Huang, M. & Chen, S. Raw data of first-principles calculations for 'Effective lifetime of non-equilibrium carriers in semiconductors from non-adiabatic molecular dynamics simulations'. Zenodo (2022); https://doi.org/10.5281/zenodo.6793099
25. Wang, S., Huang, M. & Chen, S. Effective lifetime of non-equilibrium carriers in semiconductors from non-adiabatic molecular dynamics simulations. Code Ocean (2022); https://doi.org/10.24433/CO.8344712.v1

Acknowledgements

This work was supported by the National Natural Science Foundation of China (NSFC) under grants nos. 12174060, 11991060, 12088101 and U1930402, Shanghai Academic/Technology Research Leader (19XD1421300), the Program for Professor of Special Appointment (Eastern Scholar TP2019019), the National Key Research and Development Program of China (2019YFE0118100), the State Key Laboratory of ASIC & System (2021MS006) and the Young Scientist Project of MOE Innovation Platform. X.G. was supported by the NSFC under grant no. 12188101.

Author contributions

S.C. designed the research. S.W. and M.H. performed the calculations. All authors analysed the data, discussed the results and co-wrote the manuscript.

Competing interests

The authors declare no competing interests.

Additional information

Extended data is available for this paper at https://doi.org/10.1038/s43588-022-00297-y.

Supplementary information The online version contains supplementary material available at https://doi.org/10.1038/s43588-022-00297-y.

Correspondence and requests for materials should be addressed to Shiyou Chen.

Peer review information *Nature Computational Science* thanks Audrius Alkauskas, Yuan Ping and the other, anonymous, reviewer(s) for their contribution to the peer review of this work. Primary Handling Editor: Jie Pan, in collaboration with the *Nature Computational Science* team. Peer reviewer reports are available.

Reprints and permissions information is available at www.nature.com/reprints.

Publisher's note Springer Nature remains neutral with regard to jurisdictional claims in published maps and institutional affiliations.

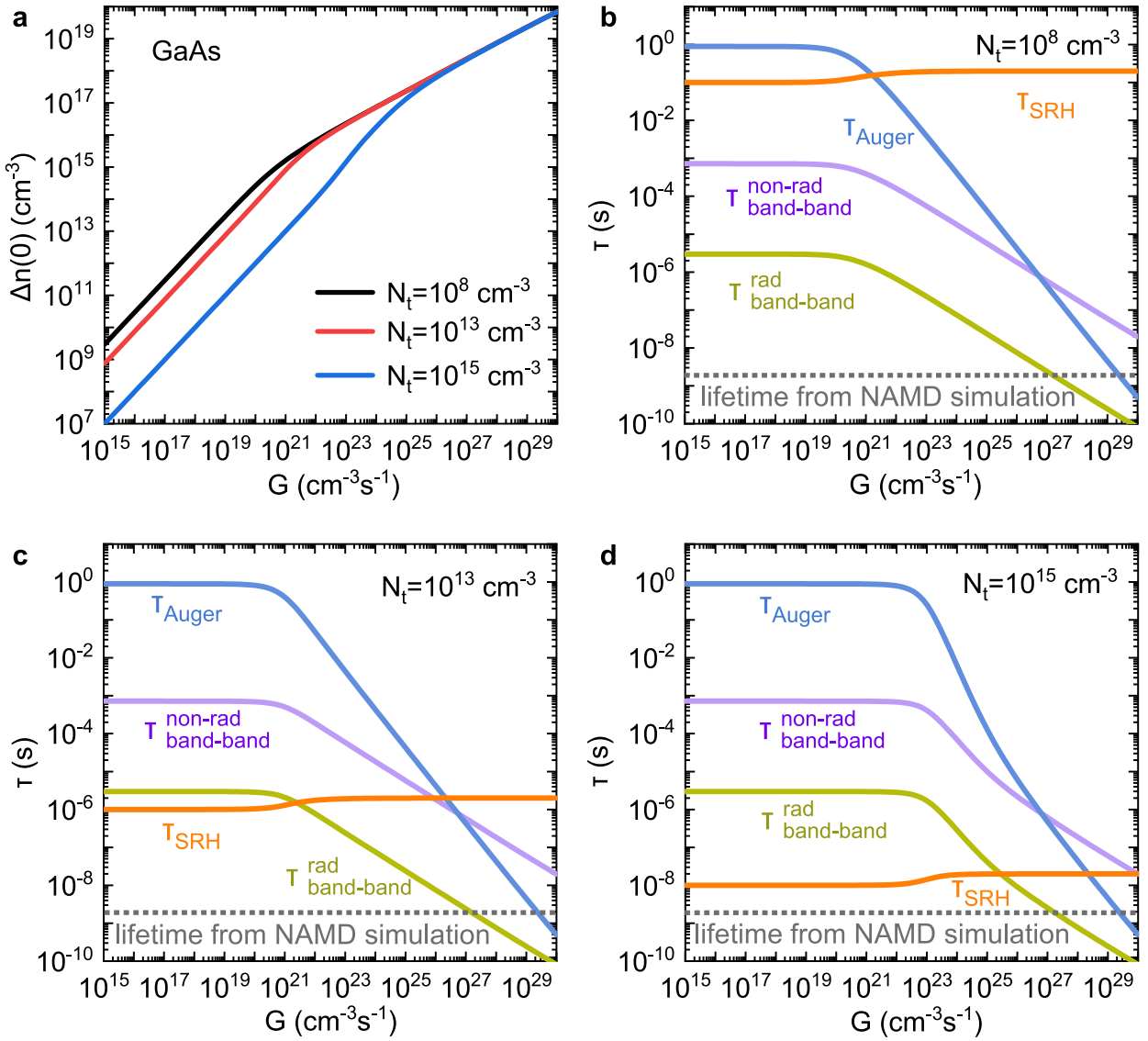

Extended Data Fig. 1 | Calculated non-equilibrium carrier density and carrier lifetime in GaAs under light illumination. a, The calculated density of non-equilibrium carriers in GaAs with varied carrier generation rate *G*. **b**-**d**, Effective carrier lifetimes for the SRH, band-to-band radiative and non-radiative, and Auger recombination in GaAs with varied *G*. The samples with different density N_t of recombination-center defects are considered, (**b**) $N_t = 10^8$, (**c**) $N_t = 10^{13}$ and (**d**) $N_t = 10^{15}$ cm^{-3}. The dashed line shows the lifetime calculated directly from the NAMD simulation of the band-to-band non-radiative recombination.

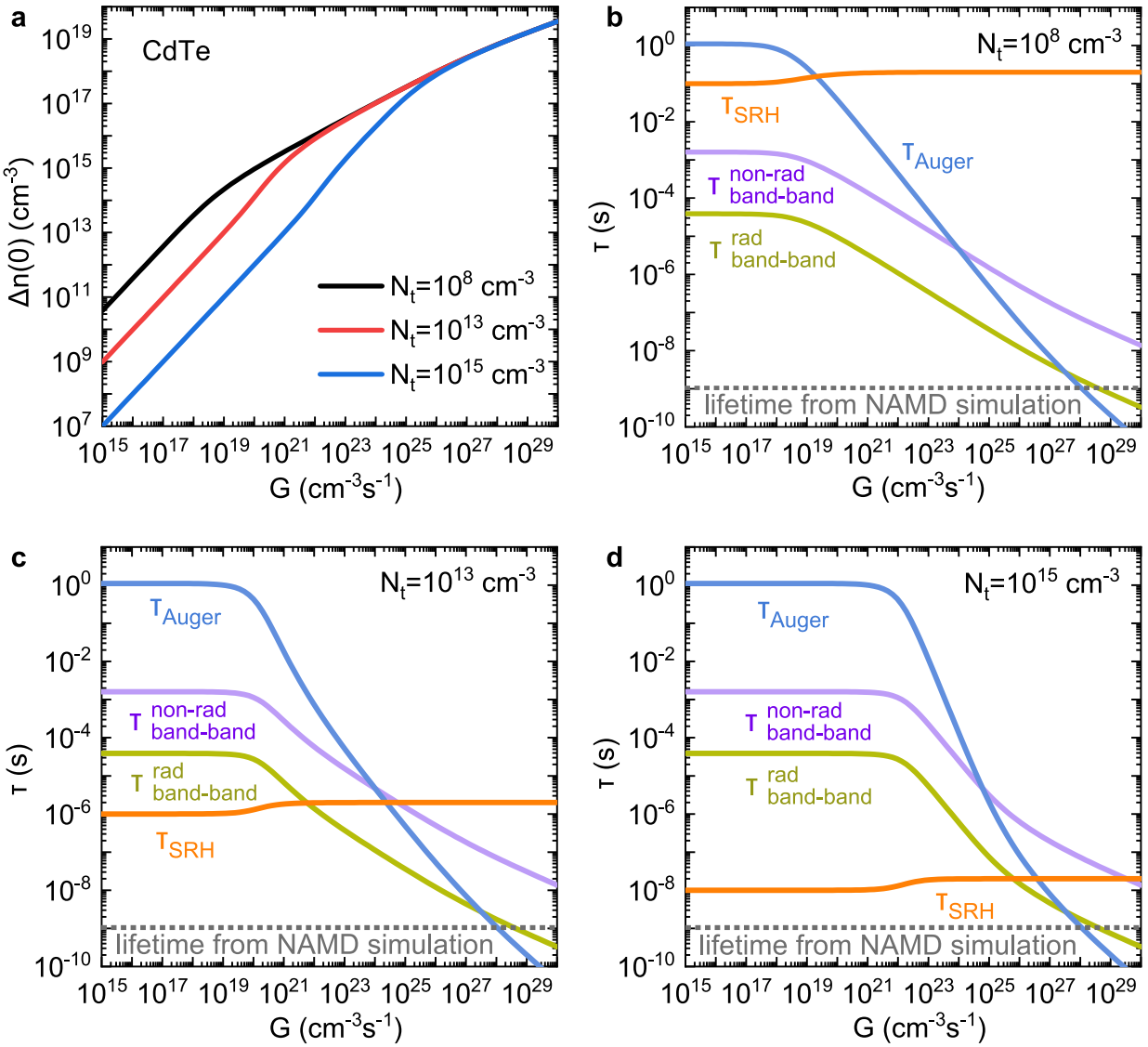

Extended Data Fig. 2 | Calculated non-equilibrium carrier density and carrier lifetime in CdTe under light illumination. a, The calculated density of non-equilibrium carriers in CdTe with varied carrier generation rate *G*. **b**-**d**, Effective carrier lifetimes for the SRH, band-to-band radiative and non-radiative, and Auger recombination in CdTe with varied *G*. The samples with different density N_t of recombination-center defects are considered, (**b**) $N_t = 10^8$, (**c**) $N_t = 10^{13}$ and (**d**) $N_t = 10^{15}\,cm^{-3}$. The dashed line shows the lifetime calculated directly from the NAMD simulation of the band-to-band non-radiative recombination.